九州工業大学学術機関リポジトリ
Kyutacar
Kyushu Institute of Technology Academic Repository

Photoelectrochemical reduction of CO2 using a TiO2 photoanode and a gas diffusion electrode modified with a metal phthalocyanine catalyst

著者	Kobayashi Katsuichiro, Lou Shi Nee, Takatsuji Yoshiyuki, Haruyama Tetsuya, Shimizu Youichi, Ohno Teruhisa
journal or publication title	Electrochimica Acta
volume	338
page range	135805-1-135805-13
year	2020-01-29
URL	http://hdl.handle.net/10228/00008704

doi: https://doi.org/10.1016/j.electacta.2020.135805

Photoelectrochemical Reduction of CO_2 using a TiO_2 Photoanode and a Gas Diffusion Electrode Modified with a Metal Phthalocyanine Catalyst

Katsuichiro Kobayashi[1], Shi Nee Lou[1,2], Yoshiyuki Takatsuji[3], Tetsuya Haruyama[3], Youichi Shimizu[1] and Teruhisa Ohno[1]**

1. Department of Applied Chemistry Section, Faculty of Engineering, Kyushu Institute of Technology, 1-1 Sensui-cho Tobata-ku, Kitakyushu, Fukuoka, 804-8550, Japan.

2. Division of Environmental Science and Engineering, Pohang University of Science and Technology (POSTECH), 77, Cheongam-ro, Nam-gu, Pohang-si, Gyeongsangbuk-do, 37673, Republic of Korea

3. Graduate School of Life Science and Systems Engineering, Kyushu Institute of Technology 2-4 Hibikino Wakamatsu-ku Kitakyushu city Fukuoka, 808-0196, Japan,

KEYWORDS Gas diffusion electrode, CO_2 reduction, photoelectrochemical system, metal-phthalocyanine, rate-limiting process

Highlights

- A TiO_2 photoanode is combined with a gas diffusion electrode modified with a Co, Ni or Sn metal phthalocyanine (MPc) catalyst and investigated for photoelectrochemical CO_2 reduction reaction (PEC CO2RR).
- NiPc catalyst shows the highest Faradaic efficiency and selectivity for PEC CO2RR to a single product, CO, at 98% whilst SnPc catalyst exhibits a high selectivity for formic acid (HCOOH) at 48% Faradaic efficiency.
- Decreasing the GDE electrolyte temperature (<11°C) through the incorporation of an ice water bath at the GDE half-cell promoted the selectivity for CO2RR.
- The selectivity for CO2RR is further enhanced by increasing the GDE half-cell sodium electrolyte concentration (<1.0 M), which reduced the electrolyte resistance.
- Voltage distribution analyses of the TiO_2 and MPc-GDE under varied applied biases show the water oxidation process at the TiO_2 photoanode is limited by a high electrode resistance whilst the cathodic CO2RR process at the MPc-GDE is limited by the activation energy of the MPc-GDE.
- In an optimized TiO_2/MPc-GDE cell using a NiPc catalyst and optimized electrolyte conditions (1.0 M Na_2SO_4 aq. electrolyte with temperature <11°C), a high PEC CO2RR efficiency to CO of 98% was achieved at a cell bias as low as 0.8 V.

Abstract

The mass transport limitations encountered in classical H-cells for electrochemical CO_2 reduction reaction (CO2RR) have spurred research in gas diffusion electrode (GDE) systems. However,

current reports on CO2RR required large biases (anode potential vs. cathode potential >-2.0 V) for high current efficiencies. In this work, we combined a TiO_2 photoanode and a GDE modified with a Co, Ni or Sn metal phthalocyanine (MPc) catalyst to reduce the external bias requirement for CO2RR. We found the Faradaic efficiencies and the selectivity of the photoelectrolysis products were influenced by (i) the metal cation (Ni, Co or Sn) coordinated to the phthalocyanine, (ii) the electrolyte temperature and concentration and (iii) the magnitude of the applied bias. In addition, analyzes of the voltage distributions between the TiO_2 photoanode and the MPc-GDE revealed the current efficiency of the TiO_2/MPc-GDE cell was limited predominantly by a high ohmic polarization loss at the TiO_2 photoanode due to an excessive thickness of the TiO_2 layer. The cathodic process at the MPc-GDE was governed by the activation energy of the electrode. The thickness of the TiO_2 photoanode was subsequently optimized for higher current efficiency. The highest Faradaic efficiency for PEC CO2RR was obtained when a NiPc catalyst was utilized as the CO2RR catalyst and the optimum cell conditions were as follows: (i) a GDE electrolyte temperature of $<11^oC$, (ii) a GDE electrolyte concentration of >1 M aq. Na_2SO_4 electrolyte solution and (iii) a TiO_2 oxidation time of 3 h. Using these optimized cell conditions and under UV illumination, the as-prepared TiO_2/NiPc-GDE cell shows a notably high CO2RR Faradaic efficiency and selectivity for CO (at 98%) and at a lowest reported cell bias of 0.8 V (anode potential vs cathode potential). This work provides an improved understanding of the cell designs of a vapor-fed CO2RR reactor based on a TiO_2/MPc-GDE photoelectrochemical system.

1. Introduction

The concentration of carbon dioxide (CO_2) in the Earth's atmosphere exceeded 410 ppm in 2018, up from 400 ppm in 2015 and 280 ppm in pre-industrial times[1]. To limit the negative impacts of CO_2 emissions on our environment, the Paris Agreement on climate change aims to hold global

mean temperature rise in this century well below 2°C[2]. This leads to an urgency to develop net CO_2 removal technologies beyond conventional approaches of utilizing bioenergy with carbon capture and storage (BECCS) and reforestation[3].

Nature relies upon green plants for CO_2 removal and carbon fixation through the photosynthesis process in green leaves. Research in artificial photosynthesis aims to recreate Mother Nature's work of photosynthesis in man-made devices, but use them to generate fuels and everyday chemicals, such as H_2, CO, formic acid (HCOOH) and other higher-order C_1 and C_{2+} hydrocarbon products. An integrated photoelectrochemical (PEC) cell for solar-driven water splitting and CO_2 reduction using a photoactive semiconductor anode and a metal catalyst modified cathode is a promising method for CO_2 reduction reaction (CO2RR) because it enables a direct conversion and storage of intermittent solar energy in chemical bonds. However, an efficient PEC CO2RR cell requires the designs and optimizations of multiple functional components to attain high efficiency and high product selectivity, for e.g., the photoanode, cathode, catalysts and electrolytes.

Table 1 summarize the oxidation and reduction half-reactions for CO2RR[4], their corresponding electrochemical potentials and Gibbs free energies derived from Nernst Equation:

Table 1: Standard Potentials (V) for CO2RR, hydrogen evolution reaction (HER) and oxgen evolution reaction (OER).

reaction	E^o (vs SHE, pH =0)	E^o (vs SHE, pH =7)	ΔG (kJ)	Eq.
$2H_2O - 4e^- \rightarrow O_2 + 4H^+$	+1.23	+0.81	+237	1
$2H^+ + 2e^- \rightarrow H_2$	0	-0.41	0	2
$CO_2 + 2H^+ + 2e^- \rightarrow CO + H_2O$	-0.11	-0.52	+20	3
$CO_2 + 2H^+ + 2e^- \rightarrow HCOOH$	-0.23	-0.64	+44	4

$CO_2 + 8H^+ + 8e^- \rightarrow CH_4 + 2H_2$	+ 0.17	-0.24	-131	5

Scheme 1a illustrates a two-electrode PEC cell for CO2RR. The four-electron water oxidation reaction (Eq. 1) proceeds at the photoanode. After CO_2 is dissolved in an aqueous electrolyte, competitive reductions of dissolved CO_2 and protons (H^+) occur at the cathode, as shown in Eq. 2-5. From the standpoint of the electrochemical reduction potential, the formation of CH_4 appears to be the most reactive due to its relatively low electroreduction potential (Eq. 5). However, the formation of CH_4 does not proceed spontaneously at low reduction potentials since it is a complex 8-electron reduction process, which requires the 2-electron reduction processes of CO_2 to occur first as intermediate steps. Among the 2-electron reduction reactions (Eq. 2-4), H_2 has the lowest reduction potential (E^o = -0.41 V vs SHE, pH=7) and is the most likely to be generated first, follows by CO (E^o = -0.52 V vs SHE, pH=7) and HCOOH (E^o = -0.64 V vs SHE)). This implies the reduction potential for CO2RR in a neutral aqueous electrolyte (pH=7) needs to be at least -0.52 V (+ kinetic overpotential). To achieve high activity and high selectivity for CO2RR, it is essential to apply a cathode with high overpotential for H^+ reduction while low overpotential for CO2RR. Although the cathode potential can be raised by increasing the applied potential across the anode and cathode, it is not possible to obtain compound formation energies above the electrical energy input. In this case, the deployment of a photoactive semiconductor that is able to convert light energy into electrical energy can raise the potential on the cathode[5]. An ideal photoanode should possess more negative photovoltage potential relative to the electroreduction potentials for CO2RR, little self-oxidation and low selectivity for peroxide formation. TiO_2 is a promising photoanode for PEC CO2RR system because of its relatively high conduction band potential, high activity and high stability for the water oxidation half-reaction[6].

The reaction rates and current densities of CO_2 electroreduction are dependent on the concentration of CO_2 in the aqueous electrolytes[7-8]. A high concentration of dissolved CO_2 at the electrode-electrolyte interface is most favorable for CO2RR[9]. However, most electrodes applied in electroreduction of CO_2, which consists of metal plates or metal granular converted thin film electrodes, have low surface areas. These coupled with the relatively low solubility of CO_2 in water under ambient conditions in conventional H-cells limit the mass transfer rate of CO_2 from the bulk solution to the solid electrode interface, which in turn, result in low current densities and low electroreduction rates for CO2RR[9]. A gas diffusion electrode (GDE) can alleviate the mass transport limitations of typical metal plates or metal granular electrodes because of their high porosity, high operating current densities and partial hydrophobicity[10]. The characteristics gas-solid-liquid (three-phase) interface of a GDE can enable homogeneous distribution of the reactants and intermediate products over the catalyst surface. These properties of GDEs are desirable for CO_2 electroreduction at the liquid-gas phase boundary. In addition, the three-phase property of a GDE is also advantageous for the separation of liquid and gaseous products upon CO2RR.

To minimize the overpotential for CO2RR, it is also important to develop efficient catalysts for incorporation on the GDE. Metal phthalocyanine (MPc) exhibits excellent catalytic properties for CO2RR[11-12]. It has a stable square planar structure and the selectivity of the adsorbed molecules can be changed by modifying the central metal cation that is coordinated to the 4 nitrogen atoms[11-12], as shown in Scheme 1e. Electrochemical CO2RR using GDEs modified with MPc catalysts and the mechanisms governing the product selectivity were investigated by Furuya et al.[11-12]. However, high applied potentials (>-2.0 V) are typically required for the electrochemical CO2RR[11].

In this work, we combine for the first time a TiO_2 photoanode with a MPc-modified GDE to overcome the mass transport limitations encountered in classical H-cell-type PEC CO2RR cells[9] and to reduce the overpotential for CO2RR, as shown in Scheme 1. The influences of the MPc central metal, Co, Ni and Sn were investigated for CO2RR product distributions and Faradaic efficiencies. To determine the rate-limiting processes governing the PEC CO2RR, the distributions of the applied biases on both the MPc-modified GDE and TiO_2 photoanode during light irradiation were also elucidated. We also investigated the optimum electrolyte concentration, electrolyte temperature and the thickness of the TiO_2 photoanode for the PEC CO2RR at the MPc-modified GDEs. Subsequently, the Faradaic efficiencies for CO2RR and H_2 evolution reaction (HER) and the applied bias to photocurrent conversion efficiency (ABPE) of an optimized TiO_2/MPc-modified GDE PEC cell were analyzed.

2. Experimental

2.1 PEC CO2RR System

The PEC CO2RR system consists of a two-electrode cell comprising a TiO_2 photoanode and a metal-catalyst modified GDE separated by a cation exchange resin film (Nafion®perfluorinated membrane, Sigma Aldrich, Nafion® NRE-212, thickness 0.0020 in), as shown in Scheme 1b. The GDE is a porous carbon sintered electrode that was placed at the interface between the CO_2 gas and the supporting electrolyte. CO_2 gas was continuously supplied to the rear side of the GDE at a constant flow rate. The unreacted CO_2 and gaseous CO2RR products were re-collected in a sample bag that was integrated at the rear side of the GDE. The half-cell potentials of the TiO_2 electrode and the MPc-GDE under an applied bias or short-circuit conditions with and

without light illumination were measured using a multi-meter and an Ag/AgCl reference electrode.

2.2 TiO_2 electrode preparation

A Ti plate (Nilaco, 99.5%, 0. 1 mm thick) was cut into the dimensions of 30 mm (l) x 60 mm (w). The Ti plates were calcined in an electric furnace at 600ºC for varied duration (0.1, 0.7, 3 and 9 h) at a ramping rate of 3ºC per min to obtain crystalline TiO_2 thin films. The presence of rutile phase TiO_2 was confirmed by X-ray diffraction (XRD), as shown by Fig. S9.

2.3 GDE preparation

The GDEs were prepared from hydrophobic carbon, hydrophilic carbon and polytetrafluoroethylene (PTFE or Teflon) by a molding process. A GDE consisting of a hydrophobic layer and a hydrophilic layer loaded with MPc catalyst was formed on a Ni mesh (Nilaco, 100 mesh, 99.9% purity, 0.1 mm thick), as illustrated in Scheme 1c.

The hydrophobic powder was prepared by mixing hydrophobic carbon (AB-7, Denki Kagaku Kogyo K.K), surfactant (Triton X-100, WAKO special grade reagent) and de-ionized water in weight ratio of 1:1:30, followed by the addition of PTFE (Teflon D-1 Daikin Ind., Ltd.) (67wt% with respect to carbon black) and then further mixing for 5 min. The as-prepared carbon paste was freeze overnight and then defreeze and filtrate. Subsequently, the particulates were dried at 120ºC for 24 h and then heat-treated in air at 280ºC for 3 h. The final hydrophobic carbon powder was micronized with a grinder.

The hydrophilic powder was prepared by mixing and stirring 36wt% hydrophilic carbon (ECP600JD, Lion Corp.), 32wt% MPc catalyst (Ni phthalocyanine (Sigma Aldrich, dye content

85%), Co phthalocyanine (Tokyo Kasei, >90% purity) and Sn phthalocyanine (Osaka Kishida, grade 1 purity)) in 100 ml of de-ionized water and 1 ml of butanol (Kantoh Chemical, special grade purity) for 2 h. This is followed by the addition of 32wt% PTFE and further stirring for 1 h. The suspension was filtered and then dried at 120ºC for 12 h. The final MPc catalyst-loaded hydrophilic carbon powder was micronized with a grinder.

To prepare the MPc-loaded GDE, the hydrophobic carbon mid-layer and the MP catalyst-loaded hydrophilic top layer were first temporarily molded on a nickel mesh using the hydrophobic and hydrophilic MPc catalyst-loaded powders, respectively. Subsequently, the main molding process was conducted at 370ºC and 20 MPa for 10 s. The final GDE is 20 mm in diameter and 2 mm in thickness, as shown in Scheme 1f.

2.4 Material Characterization

The crystalline structure of the TiO_2 thin films were characterized by X-ray diffraction (MiniFlex II, Rigaku K.K) using a Cu Kα radiation (λ=1.5405 Å) source with a potential of 30 kV and 15 mA. Scanning electron microscopy (SEM) was taken using a FESEM (JSM-6701F, JOEL) operating at an accelerating voltage 5 kV. Focus ion beam scanning electron microscopy (FIB-SEM) of the TiO_2 thin films were conducted using a FB-2000A, Hitachi.

2.5 EC and PEC CO2RR measurements

Linear sweep voltammetry (LSV) analyses and chronoamperometry of GDEs modified with different MPc catalysts were performed in a three-electrode electrochemical cell with the catalyst-modified GDE as the working electrode, Pt wire as the counter electrode, Ag/AgCl reference and a 0.1 M Na_2SO_4 aqueous electrolyte using a HOKUTO Denko potentiostat (HSV-

110). CO_2 gas or Ar gas was passed through the surface of the GDE at a flow rate of 20 cm^3 per min.

PEC CO_2 reduction reaction measurements were conducted using a two-electrode system, as shown in Scheme 1b, with MPc-modified GDE as the working electrode and TiO_2 thin film as the counter and reference electrode and a 0.1 M Na_2SO_4 aqueous electrolyte. The magnitude of the applied bias was varied between 0 to -2.0 V to determine the optimum bias for CO2RR. To enable a chemical bias to develop at the photoanode compartment, the electrolyte pH at the photoanode compartment was adjusted to pH 13 using a 1 M NaOH solution. UV illumination was provided by a 300 W Hg lamp (SX-u1501HQ360, Ushio). CO_2 gas was passed through the surface of the GDE at a flow rate of 20 cm^3 per min.

H_2 and CO gas evolutions were analyzed using a MicroGC 490, Agilent tech gas chromatograph (molecular sieve 5A column, thermal conductivity detector and He carrier gas). HCOOH was analyzed using ion chromatograph (ICS-900, DIONEX).

The Faradaic efficiencies (F.E.) for CO2RR and HER products were calculated from the ratio of the electric current required for the formation of a product to the total electric current, as shown in Eq. 6

$$F.E. = \frac{n_e \times F \times r(X)}{I_{photo}} \times 100\% \qquad \text{Eq. 6}$$

Where n_e is the number of electrons required to form a product, F is the Faraday constant, r(X) is the formation rate of a product (X) in mol/s and I_{photo} is the photocurrent (A) of the cell.

The solar-to-fuel conversion efficiencies were assessed by (i) the calculations of CO_2 reduction Faradaic efficiency and (ii) the applied bias-to-photocurrent efficiency (ABPE) as a function of applied bias. The ABPE is calculated using Eq. 7, developed by Walter et al.[6].

$$\text{ABPE (\%)} = \frac{\text{photocurrent density x (standard generation voltage} - \text{applied bias)}}{\text{power density of light irradiation}} \qquad \text{Eq.7}$$

3. Results and Discussion

3.1 Three-phase effects of GDE

To elucidate the electrochemical (EC) CO2RR properties at the gas-solid-liquid interface of a GDE modified with MPc catalyst, linear sweep voltammetry (LSV) and chrono-amperometry (CA) analyses were conducted on GDEs modified with a Co phthalocyanine (CoPc) catalyst as a model catalyst. Fig. 1a shows the current-voltage profiles of the CoPc-modified GDE cells in a CO_2 or Ar diffusion gas. The onset potential for HER at the CoPc-GDE using Ar diffusion gas occurred at -1.2 V vs Ag/AgCl. When the diffusion gas was changed from Ar to CO_2, the onset reduction potential at the CoPc-GDE shows a positive shift in reduction potential from -1.2 V vs Ag/AgCl to -0.8 V vs Ag/AgCl. The positive shift of the reduction potential implies the CoPc-GDE is favorable for CO2RR showing a lower overpotential for EC CO2RR than that for HER. Fig. 1b shows the current-time profiles of the CoPc-modified GDE cells using Ar and CO_2 diffusion gases under constant applied biases of -1.5 V vs Ag/AgCl. The electric current of the CoPc-modified GDE cell was about 43% higher in the presence of CO_2 gas than in Ar gas at 26.3 mA and 18.3 mA, respectively. Fig. 1c shows the Faradaic efficiencies of the CoPc-modified GDEs for CO and H_2 using Ar and CO_2 diffusion gases. The CoPc-modified GDE cells exhibit Faradaic efficiencies of 58.5% for CO and 37.7% for H_2 when CO_2 diffusion gas was

utilized. When Ar gas was employed as the diffusion gas, the Faradaic efficiencies were 91% for H_2 and no CO or CO_2 products were detected. The absence of carbon products when Ar diffusion gas was utilized implied the hydrophobic and hydrophilic carbon layers of the GDE are stable and do not participate in EC CO2RR. Therefore, the CO_2 diffusion gas is only the source of the carbon reduction product.

Fig. S1 ((Supporting Information (SI)) shows the locations of the gas outlets of the GDE electrochemical cell where gas measurements were taken in this study. Gaseous products (CO and H_2) and unreacted CO_2 were detected only at the gas outlet located at the gas-interphase of the GDE. No gaseous reactant and product were detected at gas outlet located above the liquid-interphase of the GDE. Using a SnPc-modified GDE (which will be discussed later), liquid formic acid (HCOOH) product was detected in the liquid electrolyte of the GDE half-cell compartment whilst CO gas was detected at the gas-interphase of the GDE half-cell. Therefore, the three-phase function of a GDE cell is verified to be useful for separating the liquid and gas products upon EC CO2RR.

3.2 Catalytic effects of MPc for electrochemical CO2RR

To examine the origin of the catalytic activity of the CoPc-modified GDE, GDE with and without CoPc catalyst modification were prepared and analyzed by LSV and CA. Upon linear voltage sweeps from -0.3 V to -1.5 V, the CoPc-modified GDE exhibit 2 to 8 times higher current densities than that of the unmodified GDEs, as shown in Fig. 1d. Using a CoPc-modified GDE, the onset reduction potential of the CoPc-GDE for EC CO2RR also shifts by +0.4 V vs Ag/AgCl from -1.2 V vs Ag/AgCl in an unmodified GDE to -0.8 V vs Ag/AgCl in a CoPc-

modified GDE (Fig. 1d). Therefore, the incorporation of a CoPc catalyst on a GDE is effective in lowering the overpotential of a GDE for CO2RR.

Fig. 1e shows the current-time profiles of the GDE cells with and without CoPc catalyst under constant applied biases of -1.5 V vs Ag/AgCl. The current of the CoPc-modified GDE cell was about 5.2 times higher than that of the unmodified GDE cell at 26.3 mA and 4.3 mA, respectively. Moreover, the product selectivity for electrochemical CO2RR also shifts from H_2 to CO using a CoPc-modified GDE compared to that of a neat GDE. The unmodified GDE exhibits Faradaic efficiencies of 65% for H_2 and 14% for CO, as shown in Fig. 1f. In contrast, the CoPc-modified GDE shows higher Faradaic efficiency for CO than H_2 at 38% for H_2 and 59% for CO, as shown in Fig. 1f.

The sequential reduction of CO_2 to CO was reported by Chen et al.[13] and Furuya et al.[11-12]. In the absence of a catalyst, the initial one-electron reduction of CO_2(aq) to form an adsorbed $CO_2^{-\cdot}$ radical intermediate on an electrode surface is an uphill reaction with a large activation barrier, as shown in Eq. S1-S2 (SI) and Scheme S1a (SI). In contrast, the second electron reduction of the $CO_2^{-\cdot}$ radical intermediate with concomitant addition of two protons to form CO and H_2O is downhill and spontaneous, as shown in Eq. S3 (SI) and Scheme S1a (SI).

Furuya et al.[11] proposed in the presence of a MPc catalyst, the adsorption of CO_2(g) on the metal cation of a MPc catalyst can not only lower the activation barrier for CO_2 reduction but also enable a direct two-electron reduction of CO_2(g) to CO(g), as shown in Eq. S4 and Eq. S5 (SI) and Scheme S1b (SI). Consequently, the employment of a MPc catalyst significantly reduces the overpotential for CO2RR, in good agreement with our current results.

3.3 Influence of the electrolyte temperature on PEC CO2RR at MPc-modified GDE

Since the solubility of CO_2 in water is dependent on electrolyte temperature[14], we investigate the effect of electrolyte temperature on the current efficiencies and product distributions of the MPC-modified GDEs. In this case, CoPc was utilized as a model MPc catalyst. To regulate the temperature of the electrolyte, we developed an alternative TiO_2-GDE PEC cell, which enabled the GDE half-cell compartment to be immersed in an ice water bath, as shown in Fig. 2a. To enable a chemical bias to develop in the PEC cell, the electrolyte solution pH at the photoanode compartment was adjusted to pH 13 whilst the electrolyte solution pH at the GDE compartment was maintained at pH 7. The effects of a chemical bias on the thermodynamic cell voltage for CO2RR is described in the SI.

Fig. 2b shows the electrolyte temperatures of the GDE half-cells under UV light illumination in the presence and absence of electrolyte cooling. Without temperature regulation, the temperature of the electrolyte at the GDE half-cell compartment increased from 30ºC to 45ºC upon light irradiation for 150 min, as shown in Fig. 2b. With the incorporation of an ice water bath at the GDE half-cell compartment, the electrolyte temperature was measured to be between 5ºC and 11ºC for a similar light irradiation period of 150 min (Fig. 2b). With no electrolyte temperature regulation, the photocurrent density of the TiO_2-GDE cell increased from 0.9 to 1.2 mA cm^{-2} after 150 min of light irradiation (Fig. 2d). With the incorporation of the ice water bath, the photocurrent density of the TiO_2-GDE cell was 50% lower at about 0.6 mA cm^{-2} for the 150 min light irradiation period (Fig. 2d.) The reduced photocurrent density is attributed to an increase in electrolyte resistance at a lower electrolyte temperature.

In term of product distributions, with no electrolyte temperature control (30-45ºC), the TiO_2-MPc-GDE cell shows higher selectivity for H_2 than CO. After 150 min of light irradiation, the Faradaic efficiencies for H_2 and CO were 58% and 32%, respectively, as shown in Fig. 2c and

2e. However, with a lower electrolyte temperature (5-11°C), the TiO_2-GDE cell shows higher selectivity for CO than H_2. After 150 min of light irradiation, the Faradaic efficiencies for H_2 and CO were 27% and 56%, respectively, as shown in Fig. 2d and 2e. The change in product selectivity to favor CO production than H_2 production with lower electrolyte temperature is likely associated with a higher solubility of CO_2 in water at a lower electrolyte temperature[14]. For example, at a pressure range below 0.1 MPa, the solubility of CO_2 in water is 0.058 M at 35°C whilst at 5°C, the solubility of CO_2 is about 2.6 times higher at 0.134 M[14]. Since the reduction of H^+ and CO_2 occurred competitively at the MPc-GDE, the higher selectivity for CO at a lower electrolyte temperature is likely due to a higher concentration of dissolved CO_2 in the electrolyte at a lower electrolyte temperature, which favors CO_2 reduction. In all electrolyte conditions, the increase in Faradaic efficiencies for H_2 and CO for the first 50 min period are likely attributed to a lower electron accumulation at the MPc-GDE during the initial illumination period.

3.4 Effects of the electrolyte concentration on PEC CO2RR at a MPc-modified GDE

The electrolyte concentration is an important factor governing the mobility of photoexcited charges at the electrode-electrolyte interface. We investigated the effects of the electrolyte concentrations of the GDE half-cell subsequently. The PEC CO2RR was analyzed in both 0.1 M and 1 M Na_2SO_4 aqueous electrolytes. As the solubility of Na_2SO_4 in water is limited at higher concentration (>1 M Na_2SO_4), PEC CO2RR was also studied in a 5 M NaCl aqueous electrolyte. Fig. 3a shows the photocurrent densities of the PEC cells in 0.1 M Na_2SO_4, 1 M Na_2SO_4 and 5 M NaCl aqueous electrolytes. An increased in electrolyte concentration from 0.1 M Na_2SO_4 to 1 M Na_2SO_4 results in a five-fold increase in photocurrent densities from 1 mA cm^{-2} to 5.1 mA cm^{-2}. Further increase in electrolyte concentration to 5 M NaCl results in an eight-fold increases in

photocurrent density to a value of 8.0 mA cm^{-2} compared to that of the 0.1 M Na_2SO_4 electrolyte solution. Fig. 3b shows the Faradaic efficiencies of the TiO_2-GDE PEC cells for CO using electrolytes of different concentrations. When the concentration of the aqueous Na_2SO_4 electrolyte was increased from 0.1 M to 1 M, the Faradaic efficiencies for CO increased from 65% to 95%. Notably, a 100% Faradaic efficiency for CO was measured when a 5 M NaCl electrolyte was utilized.

Fig. 3c shows an equivalent circuit of a GDE half-cell. The equivalent circuit demonstrates the resistance of the electrolyte solution (R-Elec) is in series with the resistance of the GDE (R-GDE). Consequently, the resistance of the electrolyte solution directly affects the electric current of the GDE PEC cell. Fig. 3d shows the relationship between the electrolyte concentration and the specific resistance of the electrolyte. The specific resistance-electrolyte concentration curve shows an exponential decrease in electrolyte resistivity when the concentration of the electrolyte is increased from 0.1 M Na_2SO_4 to 1 M Na_2SO_4 from approx. 8 Ωm to 0.2 Ωm. This implies an electrolyte concentration of at least 1.0 M is required to obtain a low electrolyte resistance for high photocurrent output.

A 2-pole-2-cell circuit of a TiO_2/CoPc-GDE system was also designed to investigate the potential drops caused by the electrolyte and membrane in the cells under light illumination and an applied bias of -1.2 V, as shown in Fig. S10 (Supporting Information). The voltages of the cells were measured directly with two Ag/AgCl reference electrodes and three voltmeters. Fig. S11 shows a schematic illustration of the potential drops caused by an electrolyte concentration of (a) 1 M aq. Na_2SO_4 and (b) 0.1 M aq. Na_2SO_4 electrolytes and across the Nafion membrane. When a high concentration (1 M) aq. Na_2SO_4 electrolyte was applied at both cells, the potential drop caused by the electrolyte was found to be negligible at 0.0047 V (11 Ω). However, the

potential drop caused by the electrolyte was significant at 0.167 V (60 Ω) when a low concentration (0.1 M) aq. Na_2SO_4 electrolyte was utilized. The potential drop caused by a low concentration (0.1 M) aq. Na_2SO_4 electrolyte is 3.5 times higher than that of the 1 M aq. Na_2SO_4 electrolyte (0.0047 V, 11 Ω). The potential drops across the Nafion membrane in both electrolyte conditions were found to be insignificant at 0.005 V for 1.0 M aq. Na_2SO_4 electrolyte and 0.004 V for 0.1 M aq. Na_2SO_4 electrolyte. Hence, the observed lower Faradaic efficiency for CO using a 0.1 M Na_2SO_4 electrolyte (F.E. = 65% for CO) compared to that of a 1 M Na_2SO_4 electrolyte (F.E. = 95% for CO) can be attributed to a large ohmic potential drop at the electrode-electrolyte interface caused by a limited conductivity of the electrolyte solution at a low electrolyte concentration.

3.5 Influence of applied voltage on photocurrent and CO2RR product distribution

The magnitude of the applied bias can influence the conduction and valence band bending of the TiO_2 semiconductor and the rate of the photoexcited charge transfer from the TiO_2 photoanode to the GDE[5]. To elucidate the effects of an applied voltage on the photocurrent and CO2RR product distribution of the TiO_2/CoPc-GDE PEC cell, the applied voltage was varied from 0 V to -2.0 V (GDE vs TiO_2) whilst the photocurrent and Faradaic efficiencies of the CO2RR products were measured. Fig. 4a shows the photocurrent (I)-voltage (V) curve of the TiO_2/CoPc-GDE PEC cell. The I-V curve shows a cubic relationship governed by $I = -3.3V^3 - 13V^2 + 5V - 0.4$, $R^2 = 0.9996$. The cubic relationship between current and voltage implies the oxidation or reduction reaction at the anode and cathode, respectively, is energy limited since the current changes exponentially with respect to the applied voltage. Fig. 4b shows the Faradaic efficiencies for H_2 and CO with respect to the applied voltages. At low applied bias of -0.2 V, the Faradaic efficiencies for H_2 and CO were 30% and 15% respectively. As the applied bias was increased

from -0.2 V to -1.0 V, the Faradaic efficiency for CO increased from 15% to 90% whilst the Faradaic efficiency for H_2 decreased from 30% to 10%. No further change in Faradaic efficiencies was observed at higher applied biases of -1.2 V to -2 V. The Faradaic efficiencies for H_2 and CO stabilized at 10% and 90% respectively in the bias range of -1.2 V to -2.0 V. These imply the optimum applied bias for efficient CO2RR is -1.2 V. An increase in voltage above -1.2 V contributes to a higher photocurrent but does not alter product selectivity.

3.6 Effects of MPc central metal cation (Ni, Co and Sn) on PEC CO2RR

Since the product selectivity for CO2RR can be potentially influenced by the nature of the metal cation of the MPc[10,11], the electrocatalytic effects of Co-, Ni- and Sn- phthalocyanines/GDEs were analyzed using the optimum GDE electrolyte temperature and concentration and, the applied bias. Fig. 5a-b shows the product concentrations, current densities and Faradaic efficiencies of Co-, Ni- and Sn-MPC/GDEs under applied biases of -1.2 V (GDE vs TiO_2) and UV illumination. CO was the predominant product when NiPc and CoPc catalysts were utilized. In the case of SnPc catalyst, HCOOH was the main product. Approx. 6150 and 6060 ppm of CO were produced using the NiPc- and CoPc-modified GDEs cells, respectively. No formic acid product was detected when NiPc and CoPc catalysts were utilized. The NiPc-GDE cell shows nearly 100% Faradaic efficiency for CO whilst the CoPc-GDE cell exhibits 86% Faradaic efficiency for CO. The SnPc-GDE cell exhibits 48% Faradaic efficiency for HCOOH, 28% Faradaic efficiency for CO and 18% Faradaic efficiency for H_2. Approx. 2200-2900 ppm of HCOOH was produced by the SnPC-modified GDE cell. The MPc-GDE were also co-modified with Au, Ag and Cu metal nanoparticles using electrodeposition methods (See SI, Table S1 for experimental methods) and investigated for PEC CO2RR. However, no significant improvement

in CO2RR product concentrations, photocurrent densities and Faradaic efficiencies were observed, as shown in Fig. S2.

Furuya et al. applied linear combination of atomic orbitals-molecular orbital (LCAO-MO) method to explain the difference in EC CO2RR product selectivity for various MPc catalysts for CO, CH_4 or HCOOH[12]. They proposed the difference in the electrolysis products can be attributed to the difference in electron configurations of the metallic atoms in the MPc. The reduction of CO_2 to CO is favored in MPcs which contains metal cations with partially filled d-shells (for e.g., in NiPc and CoPc) due to the strong electron-donating ability of the HOMO levels of theses $[MPc]^{n-}$. Upon formation of CO, the electrons in the filled $2a_{1g}$ (d_z^2) of the metal cations strongly repel the lone-pair electrons of the C atom of CO and this leads to a rapid desorption of the produced CO before further reaction can take place. However, in the case of MPc that contain metal cations with outermost s or p electrons, for e.g. in SnPc, the relatively wider LUMO band does not favor electron occupation, this hinder a direct two-electron reduction of CO_2 to CO. Instead, the reduction of CO_2 may occur in step-wise to produce HCOOH, whereby an electron is first transferred from the MPc to CO_2, to form a carbon dioxide complex, $[CO_2]^-$, follows by, a second electron transfer to generate HCOOH in the presence of H^+ ions in the solution, as shown in Fig. S3 (SI). Therefore, NiPc and CoPc catalysts show higher selectivity for CO whilst SnPc catalyst shows a higher selectivity for HCOOH. Our results are in good agreement with Furuya et al.[11].

3.7 Distribution of applied voltages across TiO_2 photoanode and GDE during PEC CO2RR

It is essential to analyze the voltage distribution mechanism across the TiO_2 photoanode and GDE upon light irradiation and applied bias in order to evaluate the rate-limiting processes governing the TiO_2 photoanode and GDE for the design of a more efficient TiO_2/MPc-GDE cell for PEC CO2RR. Fig. 6a shows the potential diagram of TiO_2 electrode and CoPc-GDE at 0 V applied bias (GDE vs TiO_2) and without light irradiation. The half-cell potentials for TiO_2 electrode and MPc-GDE were found to be +0.21 V vs Ag/AgCl, respectively. A 0.05 mA dark current was measured across the electrodes at the short-circuit conditions. Under the short-circuit conditions, the Fermi level of the TiO_2-CoPc/GDE cell is equal[5], as shown in Fig. 6a. The Fermi level potential can be indicated by the half-cell potentials of the TiO_2 and MPc-GDE, which were measured to be +0.21 V vs Ag/AgCl, respectively.

Under light irradiation of the TiO_2 photoanode while at short-circuit condition, the half-cell potentials of TiO_2 and MPc-GDE were measured to be -0.80 V vs Ag/AgCl, respectively. The decrease in half-cell potentials upon light irradiation of the TiO_2 photoanode is attributed to the photo-generation of electrons and holes at the TiO_2 electrode surface and the subsequent separation of electron-hole pairs in the depletion layer, which causes the Fermi-level of the TiO_2 semiconductor to be driven to its flatband potential[5], as shown in Fig. 6b. As the light irradiation is conducted at short-circuit conditions, the Fermi-level of the TiO_2/GDE cell is also equal. The photo-voltage gained upon illumination of the TiO_2/MPc-GDE cell can be calculated by the difference in Fermi-potentials of the dark and illuminated cells under short circuit conditions. The TiO_2/MPc-GDE cell exhibited a photo-voltage gain of 1.01 V under light illumination.

Upon application of -2.0 V bias (GDE vs TiO_2) and under light illumination, the half-cell potentials of the TiO_2 and CoPc-GDE were measured to be +0.64 V vs Ag/AgCl and -1.36 V vs

Ag/AgCl, respectively. The bias condition drives a downward band bending of the conduction and valence bands of TiO_2, this lowers the Fermi level of the TiO_2[5], as shown in Fig. 6c. However, unlike the short-circuit condition scenarios, the Fermi levels of the TiO_2 photoanode and the CoPc-GDE are not equal under an applied bias[5]. The Fermi level of the CoPc-GDE is raised by the size of the applied bias with respect to the Fermi level of the TiO_2 photoanode[5], as shown in Fig. 6c.

Fig. 6d shows the distribution of the voltages at TiO_2 photoanode and CoPc-GDE under light illumination and at different applied biases from 0 V to -2.0 V (GDE vs TiO_2). The distribution of the voltages across the TiO_2 photoanode and CoPc-GDE is asymmetrical in the presence of the light illumination and an applied bias. In the applied bias range of 0 V and -0.6 V, the distribution of the applied bias at the GDE and TiO_2 is almost equivalent (1:1). However, with increasing applied bias from -0.6 V to -2.0 V, the voltage distribution was shifted greatly towards TiO_2, as shown in Fig. 6d. For e.g., at an applied bias of -1.2 V, the ratio of voltage distributed to GDE and TiO_2 was 1: 1.8. However, at -2.0 V, the ratio widens to become 1: 2.6. The larger distribution of the applied bias to the TiO_2 photoanode than the MPc-GDE with increasing applied bias implies there is an increase in resistivity at the TiO_2 photoanode under a larger applied bias.

3.8 Rate-limiting processes governing TiO_2 photoanode and GDE

To investigate the rate-limiting processes influencing the voltage distribution to the TiO_2 photoanode and MPc-GDE, the half-cell potentials for TiO_2 and CoPc-modified GDE were modelled against the cell photocurrent. Fig. 7a shows the photocurrent-electrode potential curves for TiO_2 and CoPc-GDE and their corresponding approximated expressions. The photocurrent

(I)-electrode potential (V_{TiO2}) curve for TiO_2 exhibits a linear correlation, $I = -26V_{TiO2} - 21$, ($R^2 = 0.999$). However, for CoPc-GDE, the photocurrent (I)-electrode potential (V_{GDE}) curve shows a cubic correlation, $I = 26(V_{GDE})^3 - 83(V_{GDE})^2 - 210(V_{GDE}) - 102$, ($R^2 = 0.998$). In general, the polarization loss of an electrochemical cell can be divided into three distinct regions[15]: (i) activation polarization, (ii) ohmic polarization and (iii) concentration polarization, as shown in Fig. 7b. A cubic relationship between photocurrent and electrode potential for NiPc-GDE implies the electroreduction process at the GDE is likely limited by activation losses due to limitations in electrochemical reaction kinetics. Since the activation overpotential expressions can be derived from the Butler-Volmer equation and expressed as a Tafel equation[15], as shown in Eq. 13, the I-V_{GDE} curve for NiPc-GDE was fitted using the Tafel equation. Fig. 7c shows the Tafel plot of the NiPc-GDE and the corresponding approximate expression. The log i vs V of NiPc-GDE shows a good fit to the Tafel equation ($R^2 = 0.984$) and hence, signifies the PEC CO2RR process at the CoPc-GDE is limited by activation polarization losses.

$$\log i = \log i_0 + \frac{\alpha n}{0.059} V \qquad \text{Eq. 13}$$

Where, i = current, i_0 = exchange current (in an equilibrium state), V = applied potential, α = asymmetric parameter (distribution ratio of V) and n = reactive valence electron.

For the TiO_2 photoanode, the linear correlation between photocurrent and electrode potential (V_{TiO2}) likely implies the solar water oxidation process at the TiO_2 photoanode is limited by a high ohmic polarization loss. Fig. S4 and S5 show the equivalent circuit diagrams of the TiO_2/GDE PEC system. Table S2-5 details the resistance of each component of the cell. The contribution of resistance to the TiO_2 electrode cell compartment is in the following order: Ti ($10^{-7}\Omega m$) < Na_2SO_4 electrolyte (1M, $10^{-2}\ \Omega m$) < photo-irradiated TiO_2 ($10^0\ \Omega m$) < electric

double layer (10^3 Ωm) < non-illuminated TiO_2 (10^4 Ωm). Therefore, a non-photo-irradiated TiO_2 contributes the highest resistance to the TiO_2 electrode half-cell compartment. However, it is important to note that light radiation on a TiO_2 has an effect of lowering its resistance by 4 orders of magnitude due to the generation of photoexcited electrons and holes. To reduce the ohmic polarization loss of the TiO_2 electrode half-cell, it is essential to optimize the thickness of the TiO_2 layer for higher conductivity.

3.9 Reduction of TiO_2 electrode resistance

To measure the thickness of the TiO_2 thin films, SEM-EDS line scan analyses were conducted across the cross-sections of the TiO_2 thin films. The SEM images and SEM-EDS line scan of a TiO_2 thin film cross-section can be seen in Fig. S6 (SI). For a TiO_2 thin film that was prepared by thermal oxidation of a Ti plate at 600°C for 3 h, the SEM-EDS line scan shows the TiO_2 thin film exhibits a tri-layered structure consisting of a pure TiO_2 topmost layer (approx. 1.0 μm), a TiO_2/Ti gradient mid-zone (about 1.0 μm to 10 μm deep) and a pure Ti bottom region (>10 μm depth), which corresponds to the Ti plate. Since light ray is unable to penetrate a TiO_2 thickness that is greater than 1 μm, the TiO_2/Ti gradient mid-zone region is unlikely to participate in the photo-reaction upon light irradiation. Therefore, the high resistance of the TiO_2/Ti middle region is likely the source of the ohmic polarization loss at the TiO_2 electrode. Hence, it is necessary to optimize the thickness ratio between the TiO_2 top region and the TiO_2/Ti middle region to lower its resistance by adjusting the thermal oxidation time of the Ti plates.

Kusabiraki et al. investigated the relationship between the thickness of TiO_2 and the thermal oxidation time of Ti plates[16]. They established the thickness of TiO_2(D) is directly proportional to the square root of the Ti plate oxidation time (T), as shown in Eq. 14.

$$D \alpha \sqrt{T} \qquad \text{Eq. 14}$$

Since the thickness of the TiO_2 film is about 1.0 μm using a 3 h thermal oxidation time at 600ºC, the Ti plates were thermally oxidized for durations between 0.1 – 9 h in order to obtain TiO_2 film thicknesses between 0.2 and 2 μm. Fig. S7 shows the relationship between the TiO_2/CoPC-GDE cell photocurrent and the thermal oxidation time of the Ti plates. A maximum photocurrent of -20 mA was obtained using a TiO_2 electrode that was prepared via a 3 h thermal oxidation time in air. For thermal oxidation durations below 3 h, the thickness of the TiO_2 layer is likely insufficiently thick for high photocurrent generation. Using a thermal oxidation duration longer than 3 h likely results in a relatively thick TiO_2/Ti mid-region, which also leads to relatively lower photocurrent generation. Hence, the optimum thermal oxidation time of the Ti plate is 3 h.

Fig. S8 shows the linear sweep voltammograms (LSV) with repeated light-on and off chopping on TiO_2 photoanodes prepared at different oxidation durations. The photocurrents of the TiO_2 thin films increased with the oxidation time of the Ti plates. The TiO_2 thin film prepared using 3 h oxidation time shows the highest photocurrent. However, with longer oxidation time of 9 h, the photocurrent of the TiO_2 thin film decreases due to the increased thickness and resistance of the TiO_2 thin film. The LSV results (Fig. S8) are in good agreement with the chrono-amperometry results (Fig. S7) showing that the optimum oxidation time of the Ti plate for high photocurrent generation is 3 h.

3.10 Solar-to-fuel conversion efficiency of an optimized TiO_2/NiPc-GDE PEC cell for CO2RR

After investigating the effects of the GDE electrolyte temperature and concentration and, the thickness of the TiO_2 photoanode on light absorption and conductivity, the solar-to-fuel

conversion efficiency of a TiO_2/NiPc-GDE cell using the optimum TiO_2 electrode (3 h oxidation time) and GDE half-cell electrolyte concentration (1 M aq. Na_2SO_4 solution) and temperature (<11°C) was investigated. NiPc catalyst was utilized because NiPc shows the highest Faradaic efficiency for CO2RR (close 100% F.E. for CO), as shown in Fig. 5. Fig. 8a shows the Faradaic efficiencies for CO of the TiO_2/NiPc-GDE cell as a function of applied bias. A linear increase in Faradaic efficiencies for CO from 0% to 95% was observed as the magnitude of the applied negative bias increased from 0 V to -0.6 V. The Faradaic efficiency for CO reached a maximum of 98% from -0.6 V to -2.0 V. Fig. 8b shows the applied bias-to-photocurrent efficiency (ABPE) of the optimized TiO_2/NiPc-GDE cell. The maximum ABPE of the optimized TiO_2/NiPc-GDE cell for both CO2RR and HER is 0.19% at an applied bias of -0.8 V under UV illumination, the maximum ABPE for CO2RR is 0.18% at -0.8 V, as shown in Fig. 8b, and the Faradaic efficiency for CO is 98% at -0.8 V (Fig. 8a).

Table 2 shows a comparison of the cell potentials, current or photocurrent densities and Faradaic efficiencies of products for CO2RR of various electrochemical and PEC systems. It is important to note that most works in the literature reported a half-cell bias of their anode or cathode material for CO2RR (i.e. the anode or cathode potential vs. reference electrode). However, to evaluate the CO2RR efficiency of a system, the voltage of the full cell should be considered (i.e. the magnitude of the applied bias between the anode or photoanode and the cathode or photocathode). In order to compare the cell potential and Faradaic efficiency for CO2RR of our TiO_2/NiPc-GDE PEC cell and other systems reported in the literature, we calculated the cell potentials of various electrochemical and PEC systems by, taking into consideration, (i) the reported value of the half-cell bias for each system and, (ii) the potential of the opposite electrode was calculated by using the minimum standard voltage for H_2O oxidation or CO_2

reduction. The cell potential and performance of our cell were compared with (i) Pt/NiPc-GDE electrochemical cell[11], (ii) Pt-Cu electrochemical cell[17] and (iii) Pt-oxide-derived Au electrochemical cells[13], (iv) GaN-Cu photoelectrochemical cell[18], (v) CoPi/$BiVO_4$:Mo +4-junction photovoltaic-Cu-Au-GDE photoelectrochemical cell[19], (vi) TiO_2-Cu_2O photoelectrochemical cell[20] and (vii) Pt/Au-p-Si photoelectrochemical cell[21], as shown in Table 2. Overall, we found our optimized TiO_2/NiPc-GDE PEC cell exhibit not only the highest CO2RR efficiency of 98% for a single CO product but also at a lowest reported cell voltage of 0.8 V (anode vs cathode potential).

4. Conclusions

This work investigated for the first time a PEC CO2RR cell based on a TiO_2 photoanode and a MPc modified GDE (NiPc, CoPc and SnPc). The highest Faradaic efficiency for PEC CO2RR was obtained when a NiPc catalyst was adopted as the CO2RR catalyst and the optimum cell conditions were as follows: (i) a GDE electrolyte temperature of <11ºC, (ii) a GDE electrolyte concentration of >1M aq. Na_2SO_4 electrolyte solution and (iii) a TiO_2 oxidation time of 3 h. Using these optimized cell conditions and under UV illumination, the as-prepared TiO_2/NiPc-GDE cell showed not only a high Faradaic efficiency and a high selectivity for CO2RR (at 98% for CO) but also at a lowest reported cell bias of 0.8 V. The work also demonstrated that the modification of a GDE electrode with NiPc, SnPc or CoPc catalyst was effective in reducing the overpotential for EC CO2RR. For NiPc and CoPc, the main CO_2 reduction product was CO whilst HCOOH was the main product for SnPC. Decreasing the electrolyte temperature at the GDE cell compartment enabled a higher solubility of CO_2 in the electrolyte and a higher selectivity for CO than H_2. In addition, a high GDE electrolyte concentration (>1.0 M aq. Na_2SO_4) could reduce the electrolyte resistivity and improve the photocurrent density. Voltage distribution analysis of the TiO_2/MPc-

GDE cell showed the anodic process at the TiO_2 photoanode was limited by an ohmic polarization loss at the anode surface while the cathodic process at the MPc-GDE electrode was influenced by the activation energy of the cathode. The high resistance of the excess TiO_2 layer at the photoanode was the dominant factor that limited the distribution of the applied bias to the GDE. The low ABPE value of the TiO_2/NiPc-GDE cell at 0.19% was attributed to the wide band gap of TiO_2, which could only respond to UV light.

Scheme 1: Cartoon illustrations of (a) a two-electrode photoelectrochemical (PEC) CO_2 reduction reaction (CO2RR) cell, (b) an integrated PEC CO2RR cell, which combines a TiO_2 photoanode for generation of photoexcited charges and a Co, Ni or Sn metal phthalocyanine (MPc)-modified gas diffusion electrode (MPc-GDE) for CO2RR, note that the TiO_2 photoanode cell compartment is separated from the MPc-modified GDE cell compartment by a proton exchange resin membrane; (c) a tri-layer architecture of a MPc-modified GDE comprising a hydrophilic carbon top layer that is loaded with MPc catalysts and a hydrophobic carbon mid-layer molded onto a Ni mesh substrate and; (d) PEC CO2RR at the gas-solid-liquid (three-phase) interface of a GDE highlighting the separation of gaseous (e.g. CO) and liquid (e.g. HCOOH) products at the three-phase-interface of a GDE; (e) chemical structure of a MPc and (f) a photograph of a MPc-GDE with a diameter of 20 mm and a thickness of 2 mm.

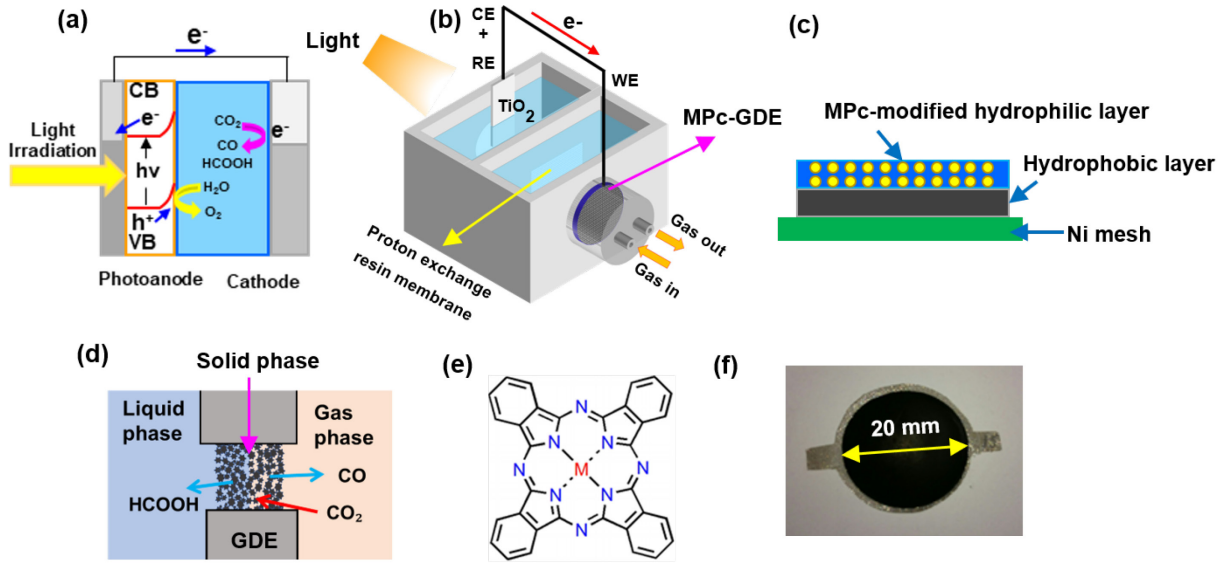

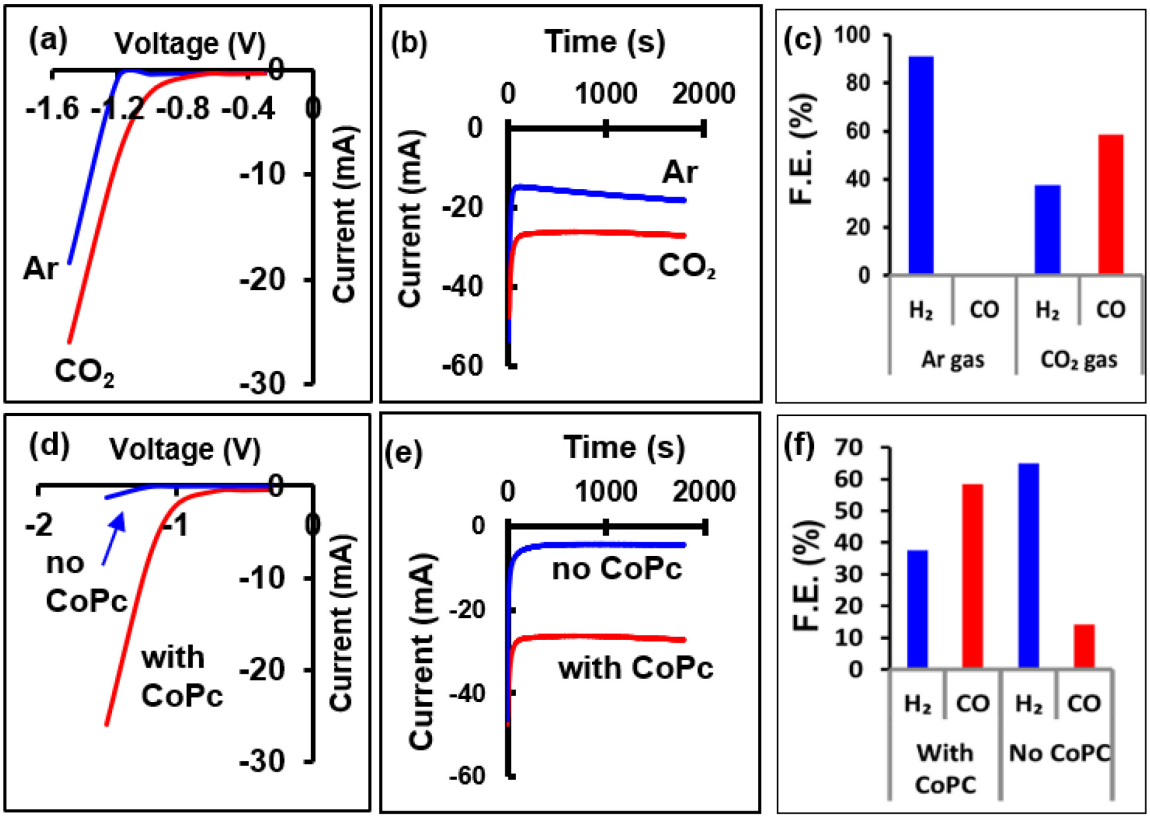

Figure 1: (a) Voltage-current curves, (b) current-time profiles and (c) Faradaic efficiencies (F.E.) of CoPc-modified GDEs for H_2 and CO in an Ar or CO_2 diffusion gas; (d) voltage-current curves, (e) current-time profiles and (f) F.E. of neat GDE (with no CoPc catalyst loading) and CoPc-modified GDE for H_2 and CO in the presence of a CO_2 diffusion gas. The LSV and CA measurements were conducted using a three-electrode cell with neat GDE or CoPc-modified GDE as the working electrode, Pt as the counter electrode and an Ag/AgCl reference electrode in a 0.1 M Na_2SO_4 aqueous electrolyte solution (pH 7); The CO_2 or Ar gas inlet gas flow rate: 20 $cm^3\ min^{-1}$. The F.E. tests were measured under constant applied biases of -1.5 V vs Ag/AgCl.

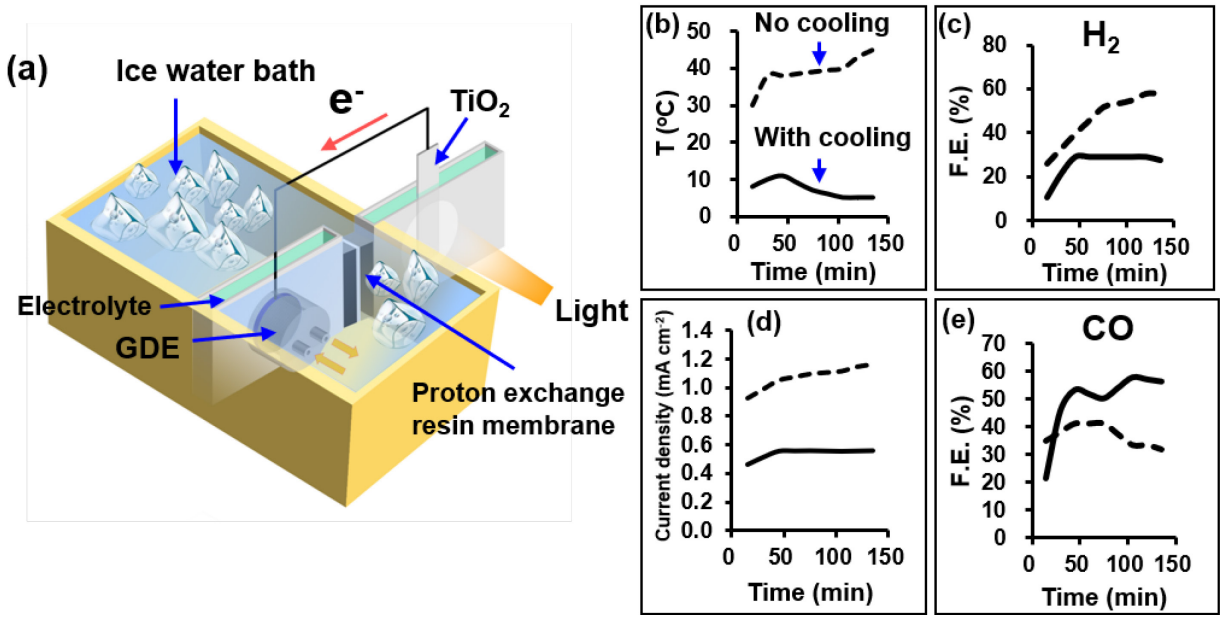

Figure 2: (a) An illustration of a TiO_2-GDE PEC cell modified with an ice water bath at the GDE half-cell compartment for electrolyte temperature regulation; (b) temperature of electrolyte during light irradiation, (c) photocurrent density-time profiles and Faradaic efficiencies for (d) H_2 and (e) CO with and without cooling of electrolyte. Two-electrode cell utilizing TiO_2 as a photoanode and CoPc-GDE as a cathode; applied bias: -1.2 V (GDE vs TiO_2); electrolyte at photoanode half-cell compartment: 0.1 M aqueous Na_2SO_4 solution (pH 13); electrolyte at GDE half-cell compartment: 0.1 M aqueous Na_2SO_4 solution (pH 7); light illumination is provided by a 300 W Hg lamp; CO_2 gas inlet gas flow rate: 20 cm^3/min; the TiO_2 photoanode was produced using 3 h oxidation time.

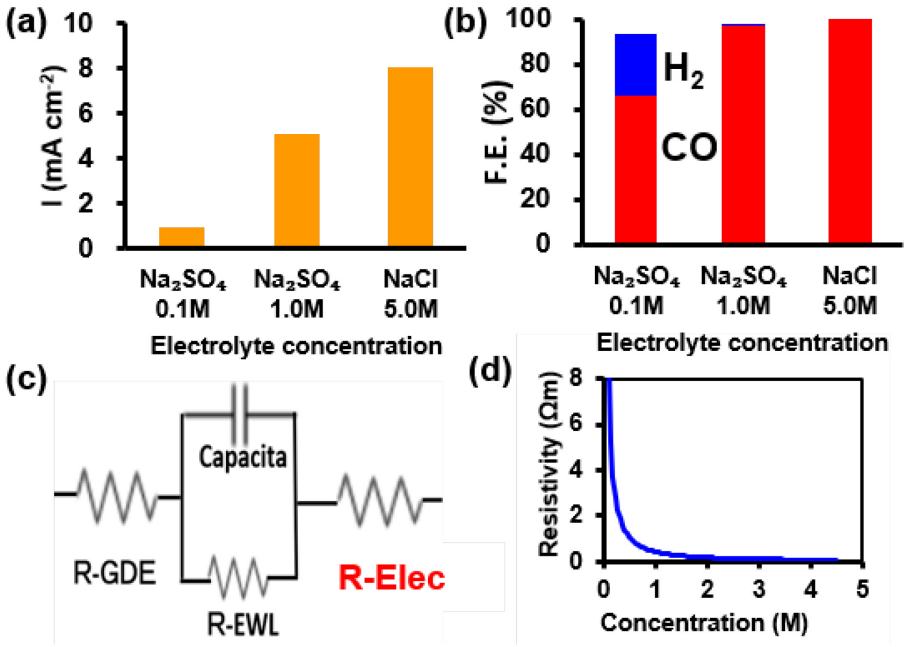

Figure 3: Influences of electrolyte concentrations on (a) photocurrent densities (I) and (b) Faradaic efficiencies for H_2 and CO; (c) equivalent circuit of a GDE half-cell, R: resistance, EWL: Electric double layer, Capacita: capacitance and Elec: electrolyte solution, and; (d) resistivity of electrolyte as a function of electrolyte concentration. Two-electrode cell utilizing TiO_2 as a photoanode and CoPc-GDE as a cathode; applied bias: -1.2 V (GDE vs TiO_2); electrolyte at photoanode half-cell compartment: 0.1 M aqueous Na_2SO_4 solution (pH 13); electrolyte at GDE half-cell compartment: 0.1 M or 1 M aqueous Na_2SO_4 solution (pH 7) or 5 M aqueous NaCl solution (pH 7); an ice-water bath for electrolyte temperature regulation of GDE half-cell was applied ($T_{electrolyte,GDE}$: <10°C); light illumination is provided by a 300 W Hg lamp; CO_2 gas inlet gas flow rate: 20 cm^3/min; the TiO_2 photoanode was produced using 3 h oxidation time.

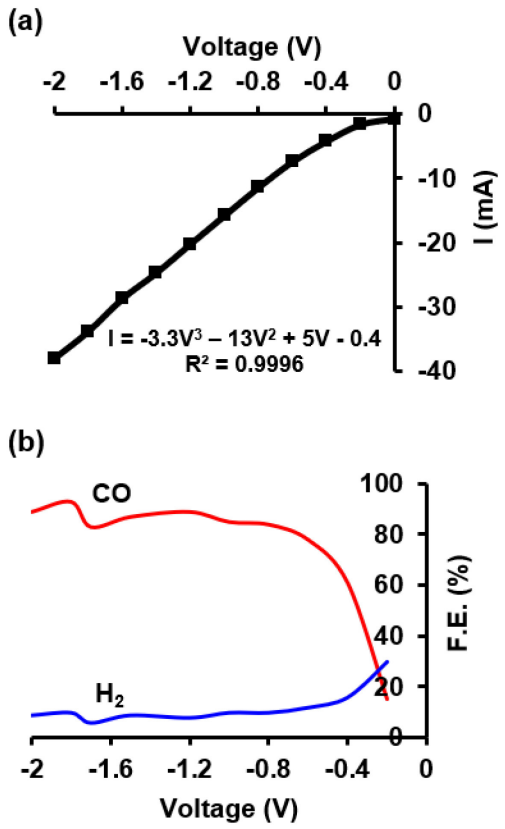

Figure 4: (a) Photocurrent (I)-voltage (V) curve of a TiO_2/CoPc-modified GDE cell with cubic curve fitting; and (b) the Faradaic efficiencies for H_2 and CO as a function of applied bias. Two-electrode cell utilizing TiO_2 as a photoanode and CoPc-GDE as a cathode; Applied bias: -1.2 V (GDE vs TiO_2); electrolyte at photoanode half-cell compartment: 0.1 M aqueous Na_2SO_4 solution (pH 13); electrolyte at GDE half-cell compartment: 1 M aqueous Na_2SO_4 solution (pH 7); an ice-water bath for electrolyte temperature regulation of the GDE half-cell was applied ($T_{electrolyte,GDE}$: <10°C); light illumination is provided by a 300 W Hg lamp; CO_2 gas inlet gas flow rate: 20 cm^3/min; the TiO_2 photoanode was produced using 3 h oxidation time.

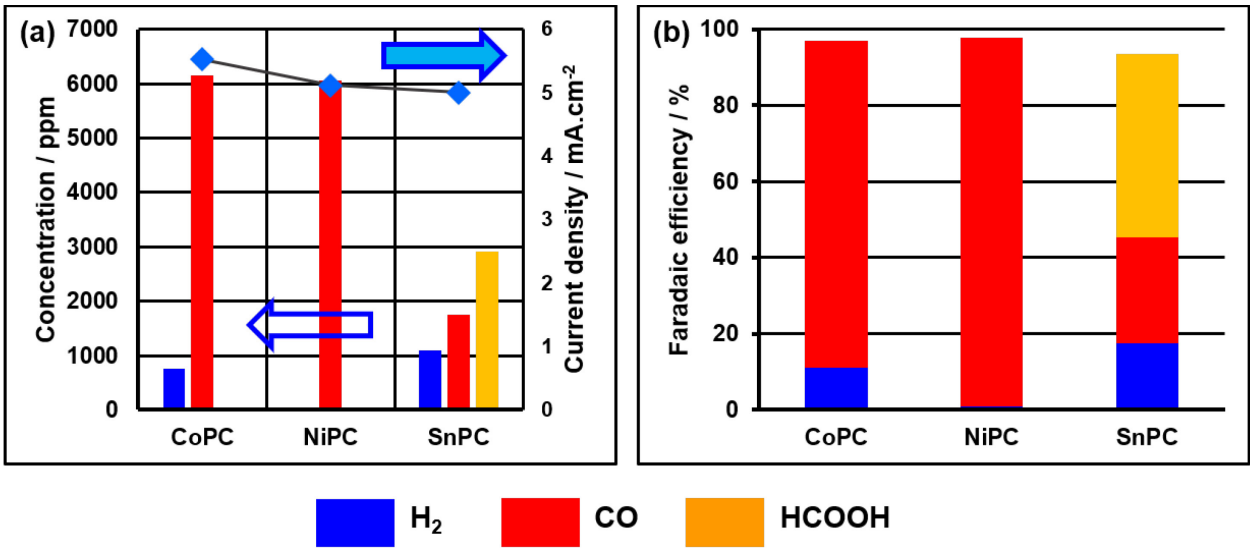

Figure 5: Light-driven two-electrode PEC CO2RR using a TiO_2 photoanode and a MPc-modified GDE electrode electrodeposited with Au, Ag or Cu cocatalyst. (a) Catalyst dependent current densities and product concentrations and; (b) catalyst dependent product's Faradaic efficiencies. Applied bias: -1.2 V (GDE vs TiO_2); electrolyte at photoanode half-cell compartment: 0.1 M aqueous Na_2SO_4 solution (pH 13); electrolyte at GDE half-cell compartment: 1 M aqueous Na_2SO_4 solution (pH 7); an ice-water bath for electrolyte temperature regulation of the GDE half-cell was applied ($T_{electrolyte,GDE}$: <10°C); light illumination is provided by a 300 W Hg lamp; CO_2 gas inlet gas flow rate: 20 cm^3/min; the TiO_2 photoanode was produced using 3 h oxidation time.

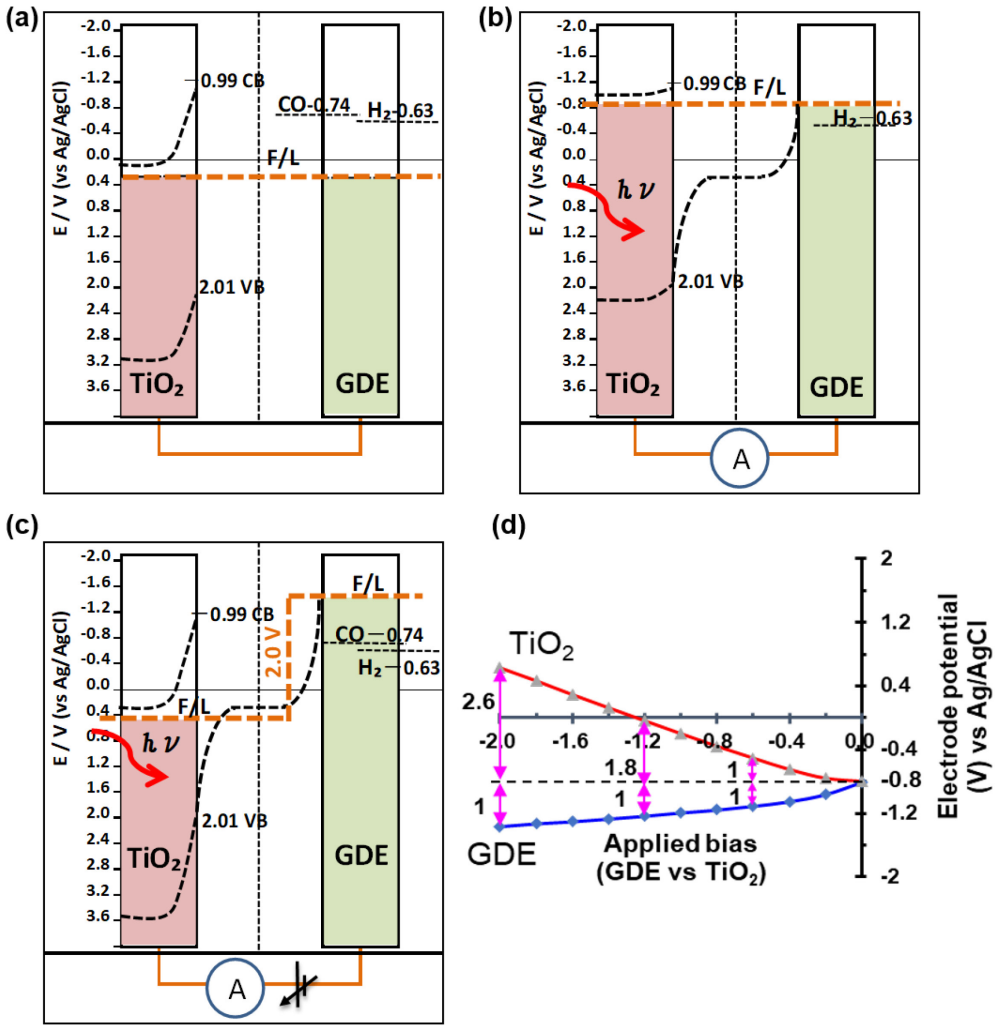

Figure 6: Potential diagrams of TiO_2 photoanode and CoPc-GDE in different conditions (a) short-circuit condition (0 V applied bias (GDE vs TiO_2)), (b) short-circuit condition and under UV-illumination of the TiO_2 photoanode (300 W Hg lamp), (c) applied bias of -2 V (GDE vs TiO_2) and under UV-illumination of the TiO_2 photoanode and (d), distribution of applied bias on TiO_2 and CoPc-GDE. Two-electrode cell utilizing TiO_2 as a photoanode and CoPc-GDE as a cathode; electrolyte at photoanode half-cell compartment: 0.1 M aqueous Na_2SO_4 solution (pH 13); electrolyte at GDE half-cell compartment: 1 M aqueous Na_2SO_4 solution (pH 7); an ice-water bath for electrolyte temperature regulation of the GDE half-cell was applied ($T_{electrolyte,GDE}$: <10°C); light illumination is provided by a 300 W Hg lamp; CO_2 gas inlet gas flow rate: 20 cm^3/min; the TiO_2 photoanode was produced using 3 h oxidation time.

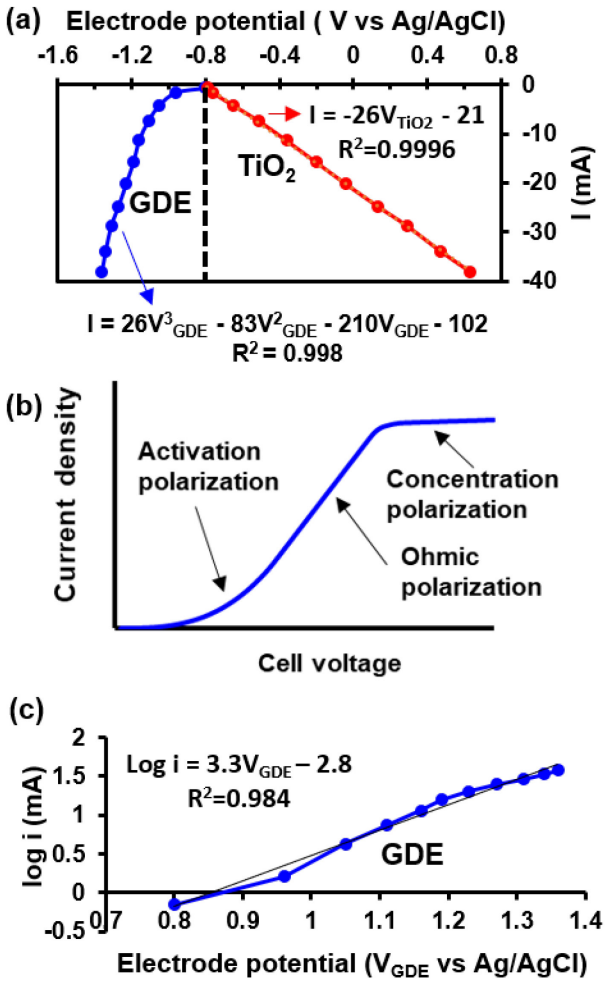

Figure 7: (a) Electrode potentials of TiO_2 photoanode and CoPc-GDE with respect to cell photocurrent and the corresponding fitting equations, (b) polarization loss curve of an electrochemical cell showing three distinct regions: activation, ohmic and concentration polarizations and (c) I-V_{GDE} curve of GDE fitted using Tafel equation. Two-electrode cell utilizing TiO_2 as a photoanode and CoPc-GDE as a cathode; electrolyte at photoanode half-cell compartment: 0.1 M aqueous Na_2SO_4 solution (pH 13); electrolyte at GDE half-cell compartment: 1 M aqueous Na_2SO_4 solution (pH 7); an ice-water bath for electrolyte temperature regulation of the GDE half-cell was applied ($T_{electrolyte,GDE}$: <10°C); light illumination is provided by a 300 W Hg lamp; CO_2 gas inlet gas flow rate: 20 cm^3/min; the TiO_2 photoanode was produced using 3 h oxidation time.

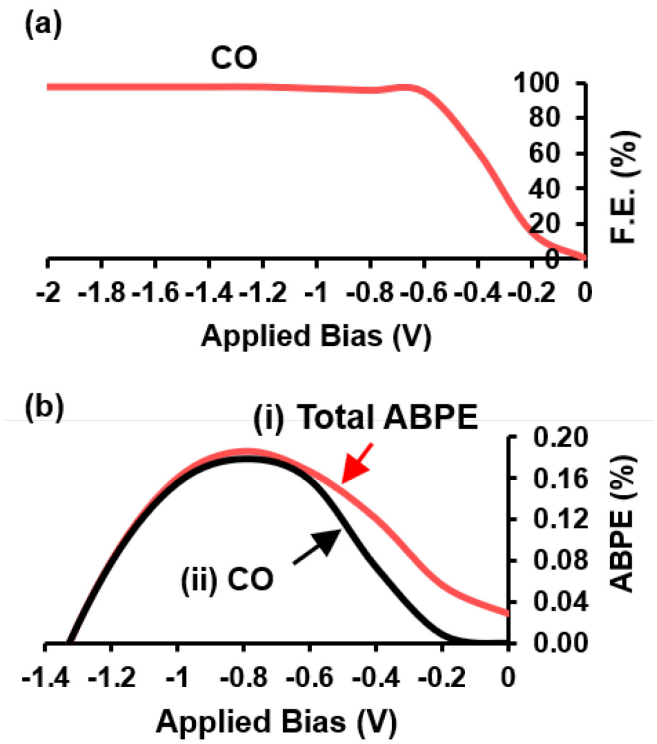

Figure 8: (a) Faradaic efficiencies for CO as a function of applied bias of the optimized TiO_2/NiPc-GDE cell under illumination and (b) applied bias-to-photocurrent efficiency (ABPE) as a function of applied bias (i) total ABPE for CO2RR and HER and (ii) APBE for CO2RR. Two-electrode cell utilizing TiO_2 as a photoanode and NiPc-GDE as a cathode; electrolyte at photoanode half-cell compartment: 0.1 M aqueous Na_2SO_4 solution (pH 13); electrolyte at GDE half-cell compartment: 1 M aqueous Na_2SO_4 solution (pH 7); an ice-water bath for electrolyte temperature regulation of the GDE half-cell was applied ($T_{electrolyte,GDE}$: <10°C); light illumination is provided by a 300 W Hg lamp CO_2 gas inlet gas flow rate: 20 cm^3/min; the TiO_2 photoanode was produced using 3 h oxidation time.

Table 2: Comparisons of various electrochemical and photoelectrochemical CO2RR systems

No.	System	Applied bias	Current	Anode potential	Cathode potential	Cell voltage (anode vs cathode)	Faradaic efficiency (%)								Ref.
			mA.cm^{-2}	V vs SHE	V vs SHE	V	CO	$HCOO^-$	CH_4	C_2H_4	MeOH	EtOH	H_2	Total CO2RR	
	Electrochemical	**Cathode vs Standard Electrode (V)**													
1	Pt anode NiPc-GDE cathode CO_2 saturated 0.5 M $KHCO_3$ electrolyte	-1.5 V vs RHE	50	+0.82	-1.1	>1.92	>95	-	-	-	-	-	<5	>95	11
2	Pt anode Cu cathode CO_2 saturated 0.1 M $KHCO_3$ electrolyte	-1.42 V vs RHE	10	+0.82	-1.42	>2.24	3.0	9.7	62.9	13	-	-	4.7	89	17
3	Pt anode Oxid- derived Au cathode CO_2 saturated 0.5 M $KHCO_3$ anolyte CO_2 saturated 0.5 M $KHCO_3$ catholyte	-0.35 vs RHE	2-4	+0.82	-0.4	>1.22	>96	-	-	-	-	-	<4	>96	13
	Photoelectrochemical	**Anode vs Standard Electrode (V)**	**Photocurrent mA.cm^{-2}**												
4	GaN photoanode Cu cathode 1 M NaOH anolyte CO_2 saturated 0.1 M $KHCO_3$ catholyte 300 W Xe lamp light source	Bias-free	1	-0.85	-0.85	0	-	3.2	-	-	-	-	-	-	18
5	CoP_i /$BiVO_4$:Mo + 4jn-CIS-PV (photoanode) Cu-Au-GDE cathode 0.1 M NaOH anolyte 0.5 M $KHCO_3$ catholyte Solar simulator AM1.5, 100 mW cm^{-2} light source	Bias-free	6.3	-1.28	-1.28	0	21.4	2.1	35	0.2	-	0	71.2	96.2	19
6	TiO_2 Photoanode Cu_2O cathode CO_2 saturated 0.1 M $KHCO_3$ electrolyte Solar simulator AM1.5, 100 mW cm^{-2} light source	0.75 V vs RHE	1.34	+1.16	-0.25	1.41	30.3	-	54.63	-	2.73	-	6.94	87.39	20
7	TiO_2 photoanode NiPc-GDE cathode 0.1 M Na_2SO_4 (pH 13) anolyte 1 M Na_2SO_4 (pH 7) catholyte 300 W Hg lamp light source	-	1.27	-0.14	-0.94	0.8	98	-	-	-	-	-	2	98	This work
		Cathode vs Standard Electrode (V)													
8	Pt anode Au/p-Si photocathode 0.1 M $KHCO_3$ anolyte CO_2 saturated 0.1 M $KHCO_3$ catholyte Tungsten-halogen lamp light source	-0.74 vs SCE	1.84	0.8	-1.21	2.01	62.2	-	-	-	-	-	9	62.2	21

ASSOCIATED CONTENT

Supporting Information.

AUTHOR INFORMATION

Corresponding Author

*Email: Prof. Teruhisa Ohno: tohno@che.kyutech.ac.jp; Dr. Shi Nee Lou: snlou@postech.ac.kr

Funding Sources

This work is supported by Japan Science and Technology Agency Advanced Catalytic Transformation Program for Carbon Utilization (ACT-C Grant Number JPMJCR12Y5)

ACKNOWLEDGMENT

The authors would like to thank Z. Zheng and Z. Teng from Yangzhou University and Kyushu Institute of Technology for their help in schematic illustrations.

REFERENCES

[1] ESRL. Trends in Atmospheric Carbon Dioxide; http://www.esrl.noaa.gov/gmd/ccgg/trends/ (accessed Feb 2019)

[2] UNCC. What is the Paris Agreement? https://unfccc.int/process-and-meetings/the-paris-agreement/the-paris-agreement (accessed Feb 2019)

[3] van Vuuren, D. P. et al. Alternative pathways to the 1.5 °C target reduce the need for negative emission technologies. Nature Climate Change 2018, 8, 391–397.

[4] The Chemical Society of Japan (2004). Chemical Handbook Fundamentals Revised 5th edition. ISBN: 4-62107314-9

[5] Nozik, A. J. Photoelectrochemistry: applications to solar energy conversion. Annual Review of Physical Chemistry 1978, 29(1), 189-222.

[6] Walter, M. G., Warren, E. L., McKone, J. R., Boettcher, S. W., Mi, Q., Santori, E. A., & Lewis, N. S. Solar water splitting cells. Chemical reviews 2010, 110(11), 6446-6473

[7] Zeman, F. Energy and material balance of CO2 capture from ambient air. Environmental Science Technology 2007, 41, 7558−7563

[8] Socolow, R., Desmond, M., Aines, R., Blackstock, J., Bolland, O., Kaarsberg, T., Lewis, N., Mazzotti, M., Pfeffer, A., Sawyer, K., Siirola, J., Smit, B., & Wilcox, J. Direct air capture of CO2 with chemicals; American Physical Society, 2011; http://www.aps.org/policy/reports/assessments/upload/dac2011.pdf.

[9] Chen, Y.; Lewis, N. S.; Xiang, C. Operational constraints and strategies for systems to effect the sustainable, solar-driven reduction of atmospheric CO2. Energy & Environmental Science 2015, 8, 3663−3674

[10] Bidault, F., Brett, D. J. L., Middleton, P. H., & Brandon, N. P. Review of gas diffusion cathodes for alkaline fuel cells. Journal of Power Sources, 187(1), 39-48, 2009

[11] Furuya, N., & Matsui, K. Electroreduction of carbon dioxide on gas-diffusion electrodes modified by metal pthalocyanines. J. Electroanal. Chem. 1989, 271, 181-191

[12] Furuya, N., & Koide, S. Electroreduction of carbon dioxide by metal phthalocyanines. Electrochimica acta, 36(8), 1309-1313, 1991

[13] Chen, Y., Li, C. W., & Kanan, M. W. Aqueous CO2 reduction at very low overpotential on oxide-derived Au nanoparticles. Journal of the American Chemical Society 2012, 134(49), 19969-19972

[14] Nippon Ekitan Corporation, technical data - solubilities of CO_2 in water, http://www.n-eco.co.jp/company/business/co2/butsu_gas.pdf (accessed June 2019)

[15] Fuel Cell Store. Polarization Curves. https://www.fuelcellstore.com/blog-section/polarization-curves (assessed June 2019)

[16] Kusabirakai, K., Sugihara, T. & Ooka, T. Oxidation behaviors of pure titanium at high temperatures in Ar-H_2O atmospheres. Iron and Steel Institute of Japan International 1992, 5, 141-148

[17] Gattrell, M., Gupta, N. and Co, A. A review of the aqueous electrochemical reduction of CO2 to hydrocarbons at copper. Journal of electroanalytical Chemistry 2006, 594(1), pp.1-19

[18] Yotsuhashi, S., Deguchi, M., Zenitani, Y., Hinogami, R., Hashiba, H., Yamada, Y. and Ohkawa, K. Photo-induced CO2 reduction with GaN electrode in aqueous system. Applied Physics Express 2011, 4(11), p.117101.

[19] Jia, Q., Tanabe, S. and Waki, I. Direct Gas-phase CO2 Reduction for Solar Methane Generation Using a Gas Diffusion Electrode with a BiVO4: Mo and a Cu-In-Se Photoanode. Chemistry Letters 2018, 47(4), pp.436-439.

[20] Chang, X., Wang, T., Zhang, P., Wei, Y., Zhao, J. and Gong, J. Stable aqueous photoelectrochemical CO2 reduction by a Cu2O dark cathode with improved selectivity for

carbonaceous products. Angewandte Chemie International Edition 2016, 55(31), pp.8840-8845.

[21] Hinogami, R., Nakamura, Y., Yae, S. and Nakato, Y. An approach to ideal semiconductor electrodes for efficient photoelectrochemical reduction of carbon dioxide by modification with small metal particles. The Journal of Physical Chemistry B 1998, 102(6), pp.974-980.